Ultrasound-activated decafluoropentane-cored and chitosan-shelled nanodroplets for oxygen delivery to hypoxic cutaneous tissues

Magnetto C; Prato M; Khadjavi A; Giribaldi G; Fenoglio I; Jose J; Gulino GR; Cavallo Federica; Quaglino E; Benitende E; Varetto G; Troia A; Cavalli R; Guiot C. Ultrasound-activated decafluoropentane-cored and chitosan-shelled nanodroplets for oxygen delivery to hypoxic cutaneous tissues. RSC ADVANCES. 4 pp: 38433-38441.
DOI: 10.1039/c4ra03524k

Ultrasound-activated decafluoropentane-cored and chitosan-shelled nanodroplets for oxygen delivery to hypoxic cutaneous tissues

Chiara Magnetto‡ a, Mauro Prato‡*bc, Amina Khadjavib, Giuliana Giribaldidi, Ivana Fenoglioe, Jithin Josef, Giulia Rossana Gulinod, Federica Cavallog, Elena Quaglinog, Emilio Benintendeh, Gianfranco Varettoh, Adriano Troiaa, Roberta Cavallii and Caterina Guiot*b

a Istituto Nazionale di Ricerca Metrologica (INRIM), Torino, Italy

b Dipartimento di Neuroscienze, Università di Torino, Corso Raffaello 30, 10125 Torino, Italy. E-mail: mauro.prato@unito.it; caterina.guiot@unito.it; Fax: +39-011-6708198; Fax: +39-011-6708174; Tel: +39-011-6708166

c Dipartimento di Scienze della Sanità Pubblica e Pediatriche, Università di Torino, Torino, Italy

d Dipartimento di Oncologia, Università di Torino, Torino, Italy

e Dipartimento di Chimica e Centro Interdipartimentale NIS, Università di Torino, Torino, Italy

f FujiFilm VisualSonics, Amsterdam, The Netherlands

g Dipartimento di Biotecnologie Molecolari e Scienze per la Salute, Molecular Biotechnology Center, Università di Torino, Torino, Italy

h Dipartimento di Scienze Chirurgiche, Università di Torino, Torino, Italy

i Dipartimento di Scienza e Tecnologia del Farmaco, Università di Torino, Torino, Italy

Ultrasound (US)-activated perfluoropentane-cored oxygen-loaded nanobubbles (OLNBs) were recently proposed as adjuvant therapeutic tools for pathologies of different etiology sharing hypoxia as a common feature (e.g. diabetes-associated chronic wounds, anaerobic infections, cancer). Here we introduce a new platform of oxygen nanocarriers, constituted of 2H,3H-decafluoropentane (DFP) as core fluorocarbon and chitosan as shell polysaccharide, and available either in liquid or gel formulations. Such oxygen-loaded nanodroplets (OLNDs) display spherical morphology, ∼700 nm diameters, cationic surfaces, good oxygen carrying capacity (without singlet oxygen generation after sterilization by ultraviolet-C rays), and no toxic effects on human keratinocytes. In vitro, OLNDs are more effective in releasing oxygen to hypoxic environments than former OLNBs, either with or without complementary US administration (f = 1 MHz; P = 5 W). In vivo, sonication of topically applied OLNDs appears essential to allow significant and time-sustained oxygen release. Taken together, the present data suggest that US-activated chitosan-shelled/DFP-cored OLNDs might be innovative, suitable and cost-effective devices to treat several hypoxia-associated pathologies of the cutaneous tissues.

1. Introduction

Tissue hypoxia, defined as reduced oxygen delivery compared to tissue demand, is a common feature of several ageing-associated skin pathologies of different etiology, including diabetes, infection, and cancer.[1–3] Human skin is a remarkably plastic organ able to sustain environmental and traumatic insult and injury throughout life. Its ability to quickly and effectively repair wounds is crucial for survival and is regulated by a complex interplay among several wound components such as differentiated cells, stem cells, cytokine networks, extracellular matrix, and mechanical forces.[4] However, when a pro-inflammatory milieu associated with hypoxia, increased proteases, and bacterial burden develops around the wound, it fails

some or all the stages which lead to healing, thus becoming chronic.5,6 Pressure ulcers, burns, diabetes-associated vasculopathies, and methicillin-resistant Staphylococcus aureus-infected wounds are some typical examples of chronic wounds, and all of them share hypoxia as a main clinical feature.1,7–9

Based on a deeper scientific understanding of oxygen physiology, and following the outcomes of randomized, prospective clinical investigations, it has been assumed that oxygen therapy in wound management is now mandatory.10 Current techniques for hyperoxygenation of wounds are hyperbaric oxygen therapy (HBOT) or topical oxygen therapy (TOT).5,10 Unfortunately, both HBOT and TOT approaches have several contra: on the one hand, HBOT is expensive, uncomfortable and even dangerous due to fire accident risks; on the other hand, TOT inadequately delivers oxygen deep into the skin to fibroblasts, keratinocytes, and inflammatory cells which need it to restore their function.5,10

Therefore, in the recent years intensive research has been performed to develop new oxygen carriers, including hemoglobin (Hb)-based carriers (dispensed as cell-free suspensions, encapsulated within vehicles, or complexed with protective enzymes).11,12 and perfluorocarbon-containing formulations (emulsions and polysaccharide-shelled micro/nanobubble suspensions).13–16

In general, perfluorocarbons are sparingly soluble molecules needed for stabilizing air bubbles in the circulation; they are extremely stable, biologically inert, and can be manufactured at very high purity.17 When injected into the bloodstream, they are excreted intact (that is, non-metabolized) in the expired air. The pulmonary elimination half-life of the F-alkanes used in ultrasound (US) contrast products is of the order of minutes.17 Extensive toxicity and absorption, distribution, and excretion data exist on neat and emulsified perfluorocarbons as a result of intensive research and development efforts on the use of perfluorocarbons in blood substitutes, liquid ventilation, and drug delivery.17 Moreover, perfluorocarbon emulsions have been shown to be toxic to cancer cells but not to healthy cells such as erythrocytes.18

Depending on their physico-chemical characteristics, perfluorocarbons vaporize at different boling temperatures, thus generating bubbles. According to the Laplace law for spherical surfaces, being the difference between the outer and the inner gas pressure in bubbles inversely proportional to their radius, the smaller the bubble radius, the higher the differential gas pressure, and the faster the gas diffusion.19

This principle has led to the development of new oxygen-loaded microbubbles (OLMBs)14,20 as well as oxygen-loaded nanobubbles (OLNBs)15,16 to counteract hypoxia in pathological tissues. Perfluorocarbon-based OLMBs have been reported to deliver clinically relevant oxygen amounts in dosages significantly lower than those used for perfluorocarbon-based emulsions.20 OLMBs shelled with chitosan and cored with perfluoropentane (PFP) were described as an efficient, biocompatible and stable oxygen delivery system in vitro.14 Recently, bubble formulations were optimized to reach the nanometer size range leading to the development of new PFP-cored OLNBs, shelled with distinct polysaccharides including chitosan and dextran.15,16 These OLNBs were shown to be uptaken either by African green monkey fibroblastoid kidney cells (Vero) or human choriocarcinoma cells (JEG-3) and to effectively inhibit HIF-1α pathway, the most common hypoxia-dependent cell signaling route. Interestingly, chitosan-shelled nanobubbles were shown capable to carry on molecules other than gaseous oxygen, such as DNA,21 suggesting intriguing exploitation in gene therapy.22

In addition, the interplay between the micro/nanobubbles and US has been investigated deeply. Injectable microbubbles (with sizes between 4 and 8 micrometer) are currently used as US contrast agents in clinical practice with licensure by health authorities.17 Furthermore, nanobubble-based contrast agents, which are small enough to leave blood vessels, have been patented to assess structures in the extravascular space and therefore image targets inaccessible to microbubbles.23 Moreover, since microbubbles greatly improve US echo signal,24 and both gas delivery and acoustic attenuation of microbubbles are enhanced by heat, OLMBs with proper dimensions and characteristics are also suitable for future applications in hyperthermic therapies.25

Interestingly, US – which is able to temporarily increase the skin permeability – can be conveniently added to enhance the delivery of such medications to, or through, the skin in a non-invasive manner commonly known as sonophoresis.16,26–28 The actual mechanism is intriguing. At first, US can induce bubble formation after acoustic droplet vaporization.29 Thereafter, bubble oscillations might lead to a stronger release mechanism due to cavitation.30 Finally, US might elicit sonoporation, temporarily enhancing skin leakage thus favoring transdermal drug release.28,31 Among the most recent applications, interesting integration of an injectable insulin-encapsulated nano-network with a focused US system has been reported to remotely regulate in vitro and in vivo insulin release in a diabetic murine model.32

In the present work, we propose an innovative platform of new oxygen nanocarriers to treat dermal and sub-cutaneous tissues. Oxygen-loaded nanodroplets (OLNDs), based on 2H,3H-decafluoropentane (DFP) as effective oxygen-storing core fluorocarbon and on chitosan as polysaccharidic shell component, were developed in liquid and gel formulations, with the latter being more suitable for topical administration. OLNDs were characterized for morphology, size, surface charge, stability, biocompatibility, oxygen content and absence of oxygen-derived species (ozone and singlet oxygen) possibly induced after UV-C sterilization. Furthermore, their effectiveness in oxygen release was assessed either in vitro or in vivo, and the role of US in eliciting such delivery throughout skin tissues was investigated.

2. Material and methods

2.1 Materials

Unless otherwise stated, all materials were from Sigma-Aldrich (St Louis, MO). Ethanol (96%) was obtained from Carlo Erba (Milan, Italy); Epikuron 200® (soya phosphatidylcholine 95%) was kindly gifted by Degussa (Hamburg, Germany); palmitic acid, DFP, PFP, chitosan (medium MW), and polyvinylpyrrolidone (PVP) were from Fluka (Buchs, CH); ultrapure water was obtained using a 1–800 Millipore system (Molsheim, France); Ultra-Turrax SG215 homogenizer was from IKA (Staufen, Germany); Delsa Nano C analyzer was from Beckman Coulter (Brea, CA); Philips CM10 instrument was from Philips (Eindoven, The Netherlands); XDS-3FL microscope was from Optika (Ponteranica, Italy); Miniscope 100 EPR spectrometer was from Magnettech (Berlin, Germany); Aeroxide P25 was from Evonik (Essen, Germany); cell culture RPMI 1640 medium was from Invitrogen, (Carlsbad, CA); cell culture Panserin 601 medium was from PAN Biotech (Aidenbach, Germany); LDO oxymeter, LCK310 ozone cuvette test kit, and DR5000 UV/Vis spectrophotometer were from Hach Lange (Salford, UK); Synergy HT microplate reader was from Bio-Tek Instruments (Winooski, VT) Zoletil 100 was from Virbac (Carros Cedex, France); Rompun was from Bayer (Leverkusen, Germany); Vevo® LAZR system for photoacoustic imaging was from Fujifilm Visualsonics (Amsterdam, The Netherlands); TINA TCM30 oxymeter was from Radiometer (Copenhagen, Denmark). BALB/c mice were bred under specific pathogen-free conditions by Fujifilm Visualsonics (Amsterdam, The Netherlands) or at the Molecular Biotechnology Center (Torino, Italy).

2.2 Preparation of oxygen carrier and control formulations

Preparation of liquid and gel formulations. To obtain a liquid formulation of OLNDs (preparation A, Table 1), 1.5 ml DFP along with 0.5 ml PVP and 1.8 ml Epikuron® 200 solved in 1% w/v ethanol and 0.3% w/v palmitic acid solution were homogenized in 30 ml water for 2 min at 24[thin space (1/6-em)]000 rpm by using Ultra-Turrax SG215 homogenizer. Thereafter, the solution was saturated with O2 for 2 min. Finally, 1.5 ml chitosan (medium MW) solution was added drop-wise whilst the mixture was homogenized at 13[thin space (1/6-em)]000 rpm for 2 min. For a liquid formulation of OLNBs the protocol developed by Cavalli and colleagues16 was applied by using PFP as a core fluorocarbon. Oxygen-free nanodroplets (OFNDs) and nanobubbles (OFNBs) were prepared according to OLND/OLNB protocols without adding O2. For oxygen-saturated solution (OSS), OLND preparation protocol was applied omitting the addiction of chitosan and DFP. To obtain gel formulations (preparations B, Table 1), 0.8 mg hydroxyethylcellulose (HEC) were solved in 20 ml water, and subsequently mixed 1[thin space (1/6-em)]:[thin space (1/6-em)]1 with OLND, OFND, OLNB, OFNB, or OSS water formulations. For more details on the structure and composition nanodroplets and nanobubbles, see Fig. 1 and Table 1.

Table 1 Composition of OLND, OFND, OLNB, OFNB and OSS formulations. Preparations A: water liquid formulations. Preparations B: 2% HEC gel formulations

Ingredients	OLNDs		OFNDs		OLNBs		OFNBs		OSS	
	Prep. A (%w/v)	Prep. B (%w/v)	Prep. A (%w/v)	Prep. B (%w/v)	Prep. A (%w/v)	Prep. B (%w/v)	Prep. A (%w/v)	Prep. B (%w/v)	Prep. A (%w/v)	Prep. B (%w/v)
chitosan (medium MW)	0,139	0,068	0,139	0,068	0,139	0,068	0,139	0,068	/	/
DFP	6,868	3,370	6,868	3,370	/	/	/	/	/	/
PFP	/	/	/	/	7,011	3,437	7,011	3,437	/	/
palmitic acid	0,015	0,007	0,015	0,007	0,015	0,007	0,015	0,007	0,020	0,010
Epikuron® 200	0,051	0,025	0,051	0,025	0,051	0,025	0,051	0,025	0,060	0,030
pvp	0,070	0,034	0,070	0,034	0,070	0,034	0,070	0,034	0,080	0,040
ethanol	3,989	1,956	3,989	1,956	3,989	1,956	3,989	1,956	4,400	2,160
filtered H2O	88,868	92,580	88,868	92,580	88,725	92,513	88,725	92,513	95,440	95,800
HEC	/	1,960	/	1,960	/	1,960	/	1,960	/	1,960
O2*	YES	YES	NO	NO	YES	YES	NO	NO	YES	YES

* O2 is merely indicated for its presence/absence in the solution (YES/NO), as it was added in excess to reach saturation; the specific O2 content was further measured during characterization, as shown in Table 2.

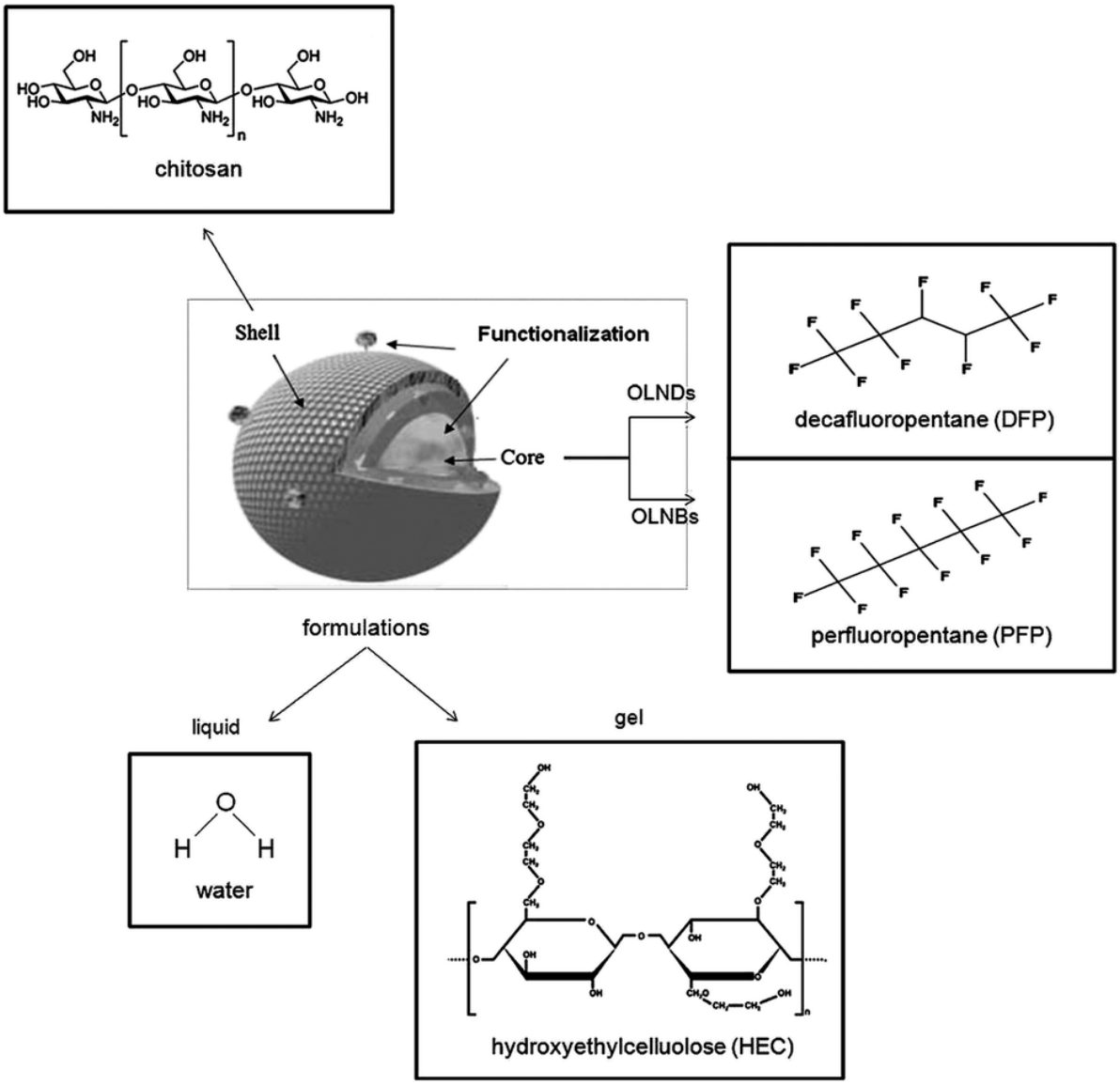

Fig. 1 Schematic structure of OLND or OLNB liquid and gel formulations.

Sterilization. OLNDs, OFNDs, OLNBs, OFNBs, and OSS were sterilized through UV-C exposure for 20 min. Thereafter, UV-C-treated materials were incubated with cell culture RPMI 1640 medium in a humidified CO2/air-incubator at 37 °C up to 72 h. No signs of microbial contamination were found when the samples were checked by optical microscopy.

2.3 Characterization of nanodroplet and nanobubble formulations

Morphology, size, particle size distribution and zeta potential. The morphology of nanodroplet and nanobubble formulations was assessed by transmitting electron microscopy (TEM) (Philips CM10) and by optical microscopy (XDS-3FL). Nanodroplet and nanobubble formulations were dropped onto a Formwar-coated copper grid and air-dried before observation.

Average diameters, polydispersity indexes, and zeta potentials of nanodroplets and nanobubbles were determined by dynamic light scattering using Delsa Nano C instrument, which portrays the particle size distribution of samples in the diameter range 0.6 nm–7 µm. Each reported value is the average of 10 independent measurements of 3 different formulations. The polydispersity index assesses the size distribution within a nanodroplet or nanobubble population. For the zeta potential determination, formulation samples were placed into an electrophoretic cell, where an electric field of approximately 30 V

cm−1 was applied. The electrophoretic mobility was converted into zeta potential using the Smoluchowski equation.33 Each sample was analyzed in triplicate.

Oxygen content. Oxygen content of OLNDs, OLNBs and OSS was estimated by adding known amounts of sodium sulphite and measuring the generated sodium sulphate, according to the reaction (1):

$$Na_2SO_3 + \frac{1}{2}O_2 \rightarrow Na_2SO_4$$

Stability. The stability of formulations stored at 4 °C, 25 °C or 37 °C was evaluated over time up to 6 months by assessing morphology, sizes and zeta potential of nanodroplets and nanobubbles by optical microscopy and light scattering.

2.4 Biocompatibility assessment

Human keratinocyte cell cultures. A long-term cell line of human keratinocytes immortalized from a 62 year old Caucasian male donor (HaCaT)34 was used to assess OLND biocompatibility. Cells were grown as monolayers in Dulbecco's modified Eagle's medium (DMEM) supplemented with 10% foetal bovine serum (FBS), 100 U ml−1 penicillin, 100 μg ml−1 streptomycin (PEN-STREP) and 2 mM L-glutamine in a humidified CO2/air-incubator at 37 °C. Before starting the experiments, cells were plated at a standard concentration (106 cells per 2 ml).

OLND cytotoxicity. The potential cytotoxic effects of OLNDs were estimated by measuring the release of lactate dehydrogenase (LDH) from HaCaT cells into the extracellular medium. Briefly, cells were incubated in 10% FBS DMEM medium for 24 h in the absence and in the presence of increasing doses (100–400 μl) of OLNDs, either in normoxic (20% O2) or hypoxic (1% O2) conditions, in a humidified CO2/air-incubator at 37 °C. Alternatively, 0.5% Triton X-100 was added to cells as an effective cytotoxic agent (positive control). Then, 1 ml of cell supernatants was collected and centrifuged at 13[thin space (1/6-em)]000g for 2 min. Cells were washed with fresh medium, detached with trypsin/EDTA (0.05/0.02% v/v), washed with PBS, resuspended in 1 ml of TRAP (82.3 mM triethanolamine, pH 7.6), and sonicated on ice with a 10 s burst. 5 μl of cell lysates and 50 μl of cell supernatants were diluted with TRAP and supplemented with 0.5 mM sodium pyruvate and 0.25 mM NADH (300 μl as a final volume) to start the reaction, which was monitored by measuring the absorbance of the sample at 340 nm (37 °C) with Synergy HT microplate reader. Both the intracellular and extracellular enzyme activities were expressed as μmol of oxidized NADH per min per well. Finally, cytotoxicity was calculated as the ratio between extracellular and total (intracellular + extracellular) LDH activities.

Human keratinocyte cell viability. Cell viability was evaluated using 3-(4,5-dimethylthiazol-2-yl)-2,5-diphenyltetrazolium bromide (MTT) assay. HaCaT cells were incubated in 10% FBS DMEM medium for 24 h without/with increasing doses (100–400 μl) of OLNDs, either in normoxic (20% O2) or hypoxic (1% O2) conditions, in a humidified CO2/air-incubator at 37 °C. Alternatively, 0.5% Triton X-100 was added to cells as an effective inhibitor of cell viability (positive control). Thereafter, 20 μl of 5 mg ml−1 MTT in PBS were added to cells for 3 additional hours at 37 °C. The plates were then centrifuged, the supernatants discarded and the dark blue formazan crystals dissolved using 100 μl of lysis buffer containing 20% (w/v) sodium dodecyl sulfate (SDS), 40% N,N-dimethylformamide (pH 4.7 in 80% acetic acid). The plates were then read on Synergy HT microplate reader at a test wavelength of 550 nm and at a reference wavelength of 650 nm.

2.5 In vitro determination of oxygen release from OLNDs

Oxygen release with US and trespassing of skin membranes. To study the ability of US-activated OLNDs to release O2 through biological membranes, a high frequency US transducer (f = 2.5 MHz; P = 5 W) was used, combined with a home-made apparatus formed by two sealed cylindrical chambers (the lower or donor chamber containing OLND, OFND, OLNB, OFNB or OSS solutions, the upper or recipient chamber containing hypoxic solution) separated by a layer of pig ear skin employed as a model of biological membrane (see Fig. 4A for details). The US transducer was alternatively switched on and off at regular time intervals of 5 min for an overall observational period of 135 min, and the oxygen concentration in the recipient chamber was monitored every 45 min by Hach Langhe LDO oxymeter. Because of the local heating caused by US, the O2 sensor was positioned laterally in the recipient chamber in order to prevent possible damage, whereas the transducer was held in a fixed position, within the donor compartment. The acoustic power of the transducer was determined through a balance's radiation force with a reflecting target, with an uncertainty of 4%.

2.6 In vivo determination of oxygen release from OLNDs

Mice. Before performing the experiments, healthy BALB/c mice were partially shaved by hair-removing cream (abdomens or hind limbs depending on the study, as described in the following paragraphs) and anaesthetized by intramuscular injection of a mixture of tiletamine/zolazepam 20 mg Kg−1 (Zoletil 100) and 5 mg Kg−1 xylazine (Rompun). All procedures were performed in accordance with the EU guidelines and with the approval of the Università di Torino animal care committee.

Measurement of oxygen transcutaneous pressure (tcpO2) with US. The shaved abdomens of three anaesthetized mice were topically treated with OLNDs and sonicated for 30 s using a home-made US equipment (f = 1 MHz, P = 5 W). Before and after treatment, tcpO2 was measured through TINA TCM30 oxymeter according to manufacturer's instructions. Notably, tcpO2 measurement is a well-consolidated technique extensively used also in clinical practice.35 All tcpO2 measurements were taken after physiological stabilization.

2.7 Statistical analysis

For every formulation, the characterization was performed in triplicate on ten independent preparations, and results are shown as means ± SD (light scattering and oxygen measurement) or as a representative image (TEM and optical microscopy). Results from cell studies (LDH and MTT) are shown as means ± SEM from three independent experiments. Results from oxygen release studies are shown as means ± SD (release with US either in vitro or in vivo) from three independent experiments or mice. SD or SEM were respectively used for descriptive or inferential information, as previously reviewed.36 All data were analyzed by Student's t test (software: Fig. P for Windows, Fig. P Corporation, Hamilton, ON, Canada) or by a one-way Analysis of Variance (ANOVA) followed by Tukey's post-hoc test (software: SPSS 16.0 for Windows, SPSS Inc., Chicago, IL).

3. Results

3.1 Characterization of OLND formulations

After manufacturing, OLND properties were challenged by comparison with several control preparations including OLNBs, oxygen-free nanodroplets (OFNDs), oxygen-free nanobubbles (OFNBs), and oxygen-saturated solution (OSS), all prepared in liquid (water) or gel (2% HEC) formulations (see Table 1). OLNDs and control preparations were characterized for: (i) morphology, by optical microscopy and TEM; (ii)

average diameters, particle size distribution, polydispersity index and zeta potential, by dynamic light scattering; and (iii) oxygen content through a chemical assay. Results are shown in Table 2 and Fig. 2.

Table 2 Physical-chemical characterization of OLNDs, OFNDs, OLNBs, OFNBs and OSS

	Outer shell polysaccharide	Inner core fluorocarbon	fluorocarbon boiling point	O_2 content (g/ml+SD)		diameters (nm+SD)	polydispersity index	zeta potential (mV+SD)
				before UV	after UV			
OLND	chitosan	DFP	51 °C	0,46 ± 0,01	0,45±0,01	726,55 ± 123,07	0,24	+35,38 ± 1,00
OFND	chitosan	DFP	51 °C	/	/	332,70 ± 101,10	0,11	+34,97 ± 1,00
OLNB	chitosan	PFP	32 °C	0,45 ± 0,01	0,44 ± 0,01	745,20 ± 117,89	0,19	+39,20 ± 1,00
OFNB	chitosan	PFP	32 °C	/	/	320,40 ± 100,90	0,10	+38,65 ± 1,00
OSS	/	/	/	0,41 ± 0,01	0,40 ± 0,01	/	/	/

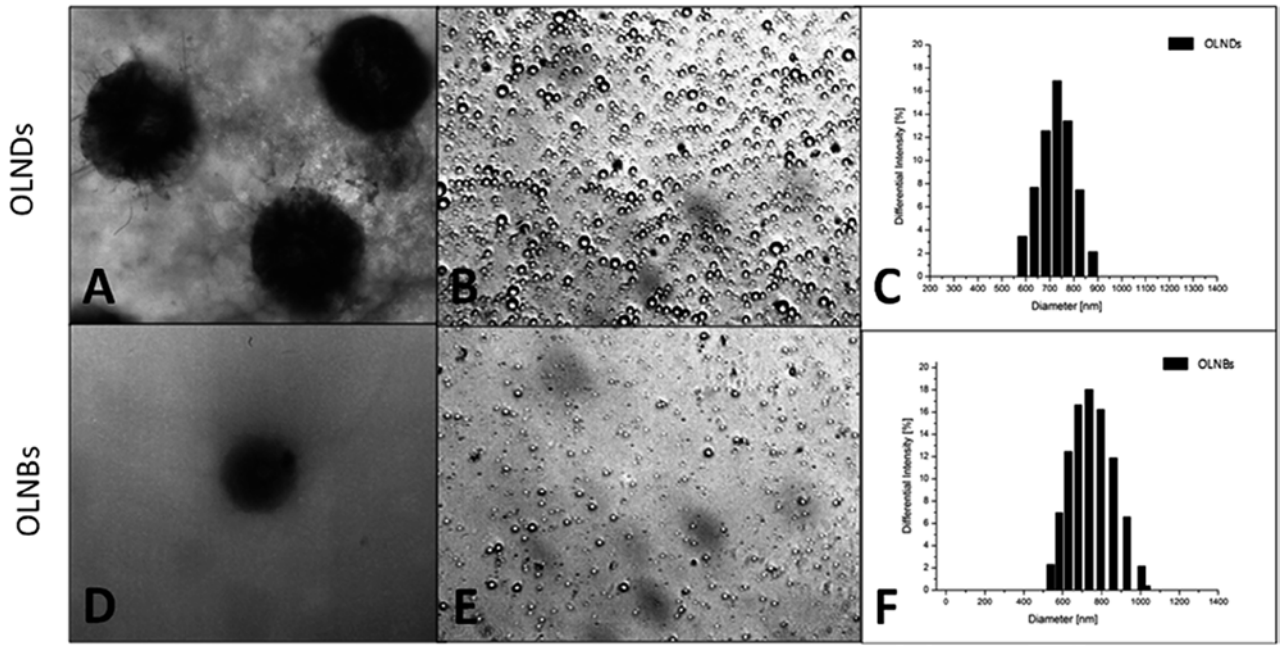

Fig. 2 OLND and OLNB morphology and size distribution. OLND and OLNB water formulations were checked for morphology by TEM or by optical microscopy and for size distribution by light scattering. Results are shown as representative images from ten different preparations for each formulation. (Panel A) TEM image of OLNDs. Magnification: 15[thin space (1/6-em)]500×. (Panel B) Optical microscopy image of OLNDs. Magnification: 630×. (Panel C) OLND size distribution. (Panel D) TEM image of OLNBs. Magnification: 52[thin space (1/6-em)]000×. (Panel E) Optical microscopy image of OLNBs. Magnification: 630×. (Panel F) OLNB size distribution.

Either nanodroplets or nanobubbles displayed spherical shapes and nanometer sizes, with average diameters ranging from ~720 nm (OLNDs) to ~740 nm (OLNBs) for oxygen-loaded carriers and from ~320 nm (OFNBs) to ~330 nm (OFNDs) for oxygen-free carriers. Moreover, nanodroplets and nanobubbles displayed cationic zeta potentials ranging from ~+35 mV for oxygen-loaded carriers to ~+40 mV for oxygen-free carriers.

OLNDs also displayed a good oxygen-storing capacity of about 0.45 g ml−1 of oxygen. Such an amount was comparable with that of OLNBs or OSS, thus justifying the use of similar volumes of OLND, OLNB and OSS preparations in further experiments testing oxygen release abilities.

Since OLNDs were sterilized through a 20 min UV-C irradiation, the possible generation of ozone and singlet oxygen was also investigated (see ESI, Fig. S1†). As emerged from analysis through a spectrophotometric assay and EPR spectroscopy, no ozone and singlet oxygen generation was detected in OLNDs after UV-C treatment.

3.2 OLND biocompatibility assessment

OLND toxicity was evaluated by testing in vitro cultures of human HaCaT keratinocytes. As shown in Fig. 3 (Panel 3A: LDH assay; Panel 3B: MTT assay), increasing volumes of OLND suspensions (100–400 µl/2 ml cell culture medium) were not toxic in normoxic conditions (20% O2), and eventually improved keratinocyte viability in hypoxic conditions (1% O2). As expected, 0.5% Triton X-100, an effective cytotoxic agent employed as positive control, induced 100% cell death (not shown).

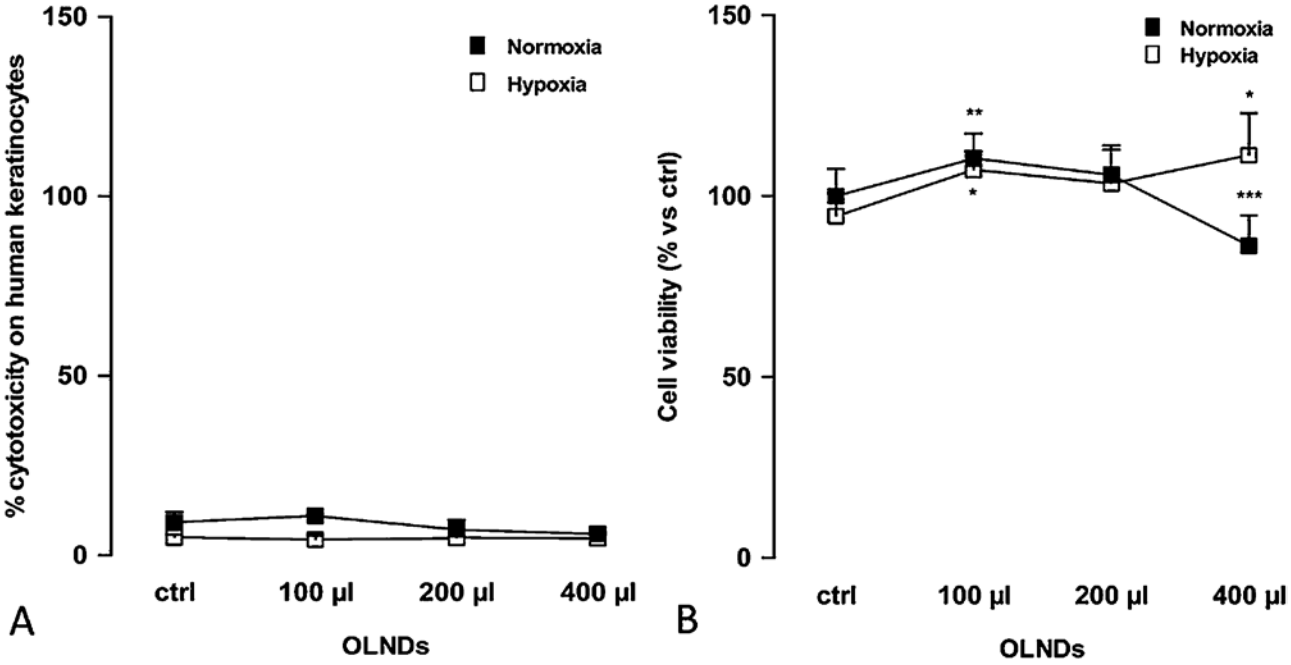

Fig. 3 Lack of OLND toxicity on human keratinocytes. Human keratinocytes (106 cells per 2 ml DMEM medium supplemented with 10% FCS) were left untreated or treated with different doses (100–400 µl) of OLNDs for 24 h in normoxia (20% O2; white-squared curve) or hypoxia (1% O2; black-squared curve). Thereafter, OLND cytotoxicity was measured through LDH assay (Panel A), and HaCaT cell viability by MTT assay (Panel B). Results are shown as means ± SEM from three independent experiments. Data were also evaluated for significance by Student's t test. (Panel A) Versus normoxic untreated cells: p not significant. (Panel B) Versus normoxic untreated cells: * $p < 0.05$; ** $p < 0.01$; *** $p < 0.005$.

3.3 In vitro oxygen release from US-treated OLNDs

In vitro OLND abilities to release oxygen were evaluated both without (see ESI, Fig. S2) or with complementary US administration (see Fig. 4). The ability of high frequency US to trigger OLND trespassing of the dermal layer and to subsequently enhance oxygen release was tested in vitro by using a home-made apparatus consisting of two sealed cylindrical chambers (oxygen-donor and oxygen-recipient, respectively) separated by a layer of pig ear skin (see Fig. 4A). Oxygen delivery from OLNDs, as well as OLND ability to trespass biological membrane after sonication were compared either to water or gel (2% HEC) formulations of OFNDs, OLNBs, OFNBs, and OSS. Results are shown in Fig. 4B and C (Panel 4B: water formulations; Panel 4C: 2% HEC formulations). US highly improved the ability of both liquid and gel OLND formulations to cross the pig skin membrane and to release oxygen into the hypoxic chamber, being such oxygen release (~0.35–0.45 mg L−1) significantly larger than that obtained from OFNDs, OLNBs, OFNBs, and OSS formulations.

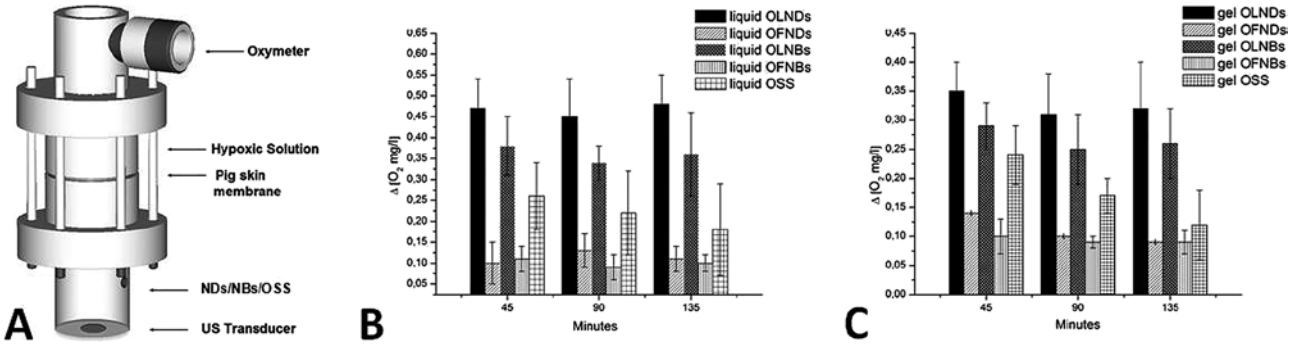

Fig. 4 US-activated OLND oxygen release and sonophoresis through skin membranes in vitro. US abilities to induce sonophoresis and oxygen release from OLND and control liquid or gel formulations were evaluated by using a home-made apparatus with two sealed cylindrical chambers (lower chamber: OLNDs, OFNDs, OLNBs, OFNBs or OSS; upper chamber: hypoxic solution) separated by a layer of pig ear skin. The US transducer (f = 2.5 MHz; P = 5 W) was alternatively switched on and off at regular time intervals of 5 min for an overall observational period of 135 min, and oxygen concentration was monitored in the recipient chamber every 45 min by Hach Langhe LDO oxymeter. (Panel A) Schematic structure of the home-made apparatus employed in the experiments. (Panel B) Sonophoresis and oxygen release from US-activated liquid (water) formulations. Results are shown as means ± SD from three independent experiments. Data were also evaluated for significance by ANOVA. Versus OLND formulation: $p < 0.04$. (Panel C) Sonophoresis and oxygen release from US-activated gel (2% HEC) formulations. Results are shown as means ± SD from three independent experiments. Data were also evaluated for significance by ANOVA. Versus OLND formulation: $p < 0.02$.

3.4 In vivo oxygen release from US-treated OLNDs

In vivo OLND abilities to release oxygen were evaluated both without or with complementary US administration. Surprisingly, as emerged by investigation through photoacoustic imaging, OLNDs did not appear more effective than OSS and OFNDs in enhancing mouse oxy-Hb levels in the absence of US complementary administration (see ESI, Fig. S3†). Therefore, the potential of high frequency US to improve tissue oxygenation by OLNDs was evaluated. The shaved abdomens of five anaesthetized mice were topically treated with OLNDs, sonicated for 30 s, and monitored for 15 min through transcutaneous oxymetry. As shown in Fig. 5, US effectively promoted transdermal oxygen delivery in a time-sustained manner for all the observational period.

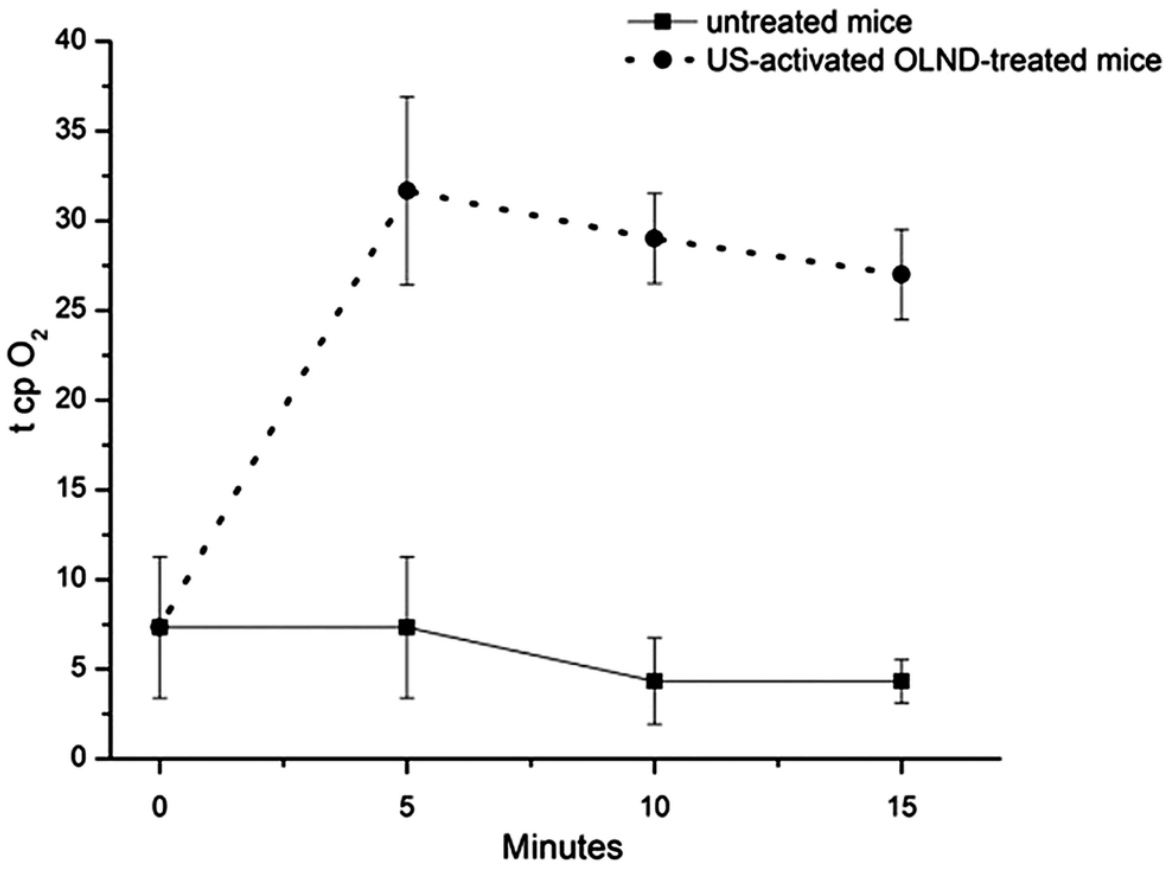

Fig. 5 Topical treatment with US-activated OLNDs effectively enhances tcpO2 in vivo. Shaved abdomens of anaesthetized mice were topically treated with OLND gel formulation and sonicated for 30 s using a home-made US equipment (f = 1 MHz; P = 5 W). Before and after treatment, tcpO2 was monitored every 5 min for 15 min through TINA TCM30 oxymeter. Data are shown as means ± SD of three mice. Results were also analyzed for statistical significance by Student's t test. Versus untreated mice: $p < 0.03$.

4. Discussion

In the present work we aimed at outdoing OLNB technology by developing a new platform of nanocarriers, namely OLNDs, which displayed higher efficiency in gas delivery than former OLNBs without losing their favorable properties (e.g. nanometer size range, stability, sensitivity to US, lack of toxicity, low manufacturing costs, ease of scale-up). The major novelty of OLNDs is the oxygen-storing core structure consisting in DFP. Unlike PFP, the gaseous fluorocarbon present in the nanobubble core, DFP is liquid at body temperature and for this reason the new nanocarriers are actually called nanodroplets. Nonetheless, DFP still keeps good oxygen-solubilizing capabilities as for PFP.37,38

On the other hand, chitosan was chosen to build the polysaccharidic shell of OLNDs. This polysaccharide is a positively charged, partially deacetylated form of chitin, a natural substance found abundantly in the exoskeletons of insects and the shells of crustaceans.39,40 The repeating units of chitosan are β(1–4)-linked glucosamines, thus it contains a large number of hydroxyl- and amino-groups providing several possibilities for derivatization or grafting of desirable bioactive groups.41,42 Chitosan also displays high biocompatibility,40,43 healing capabilities,44 anti-cancer activity45 and anti-microbial properties43 against some bacteria (e.g. methicillin-resistant Staphylococcus aureus)46 and fungi (e.g. Candida albicans).47 Due to these characteristics, it has been investigated for use in several biomedical applications, including wound dressings43 and drug carriers.42

Either nanodroplets or nanobubbles displayed spherical shapes and nanometer sizes, with average diameters ranging from ∼720 nm (OLNDs) to ∼740 nm (OLNBs). The slightly larger size of nanobubbles with respect to nanodroplets appears to be a likely consequence of the chosen fluorocarbon for the inner core. Both OLND and OLNB formulations are prepared at room temperature; however, PFP and DFP are characterized by different hydrophobicity, surface tension, and boiling point (32 °C and 51 °C, respectively).37,38 Therefore, at room temperature PFP is nearer to boil than DFP, thus provoking higher expansion of OLNB liquid inner core with respect to OLNDs, and leading to an increase of the nanobubble radius.

Moreover, nanodroplets and nanobubbles displayed cationic zeta potentials ranging from ∼+35 mV for oxygen-loaded carriers to ∼+40 mV for oxygen-free carriers. These values implicate that OLNDs are physically stable as a consequence of the electrostatic repulsion of the polymer chains. Indeed, the zeta potential measures charge repulsion or attraction between particles and is a fundamental parameter to determine nanoparticle physical stability, with zeta potentials lower than −30 mV or higher than +30 mV being generally required for physical stability of colloid systems.33 Consistently, further monitoring of sizes and zeta potentials of OLNDs confirmed their physical stability over time (not shown). The cationic surfaces were a clear consequence of the presence of chitosan, which is positively charged, in the shell.39,40 Interestingly, it has been proposed that surface-charged nanoparticles are exquisitely suitable for topical treatment, as surface charges enhance nanoparticle interaction with skin and improve their therapeutic effect on inflamed cutaneous tissues, either without48 or with concomitant US treatment.49 In particular, cationic nanoparticles are generally recommended for topical treatment due to the anionic nature of the skin.50,51

OLNDs also displayed a good oxygen-storing capacity (0.45 g ml−1), not accompanied by the generation of cytotoxic oxygen-derived reactive species such as ozone and singlet oxygen after UV-C sterilization, a well-established and effective procedure to kill viruses, bacteria, and fungi.52–55 The absence of singlet oxygen production appears extremely reassuring, as it could adversely alter several crucial biomolecules including DNA, proteins and lipids, leading to cytotoxicity and/or disease development.56,57 The potential toxicity of OLNDs was also excluded by testing in vitro cultures of human HaCaT keratinocytes, a skin cell line immortalized from a 62 year old Caucasian male donor.34 This specific cell line was chosen since hypoxia-associated pathologies of dermal tissues such as chronic wounds are more frequent in the elderly.58 Additionally, hypoxia-dependent regulation of keratinocyte proteases associated with wound repair processes, e.g. matrix metalloproteinases, is strongly influenced by the donor's age.59 According to our results, OLND suspensions were not toxic in normoxic conditions (20% O2) and eventually improved keratinocyte viability in hypoxic conditions (1% O2).

Thereafter, OLND abilities to release oxygen were evaluated both in vitro and in vivo. Intriguingly, OLNDs released larger amounts of oxygen than OLNBs and OSS in a time-sustained manner in vitro. However, in vivo experiments did not reproduce these promising results. Indeed, as emerged by analysis through photoacoustic imaging – an innovative hybrid imaging technique based on the light absorption and the acoustic transmission properties of tissues that measures blood oxygen saturation and total Hb concentration60–62 – OLNDs did appear more effective than OSS and OFNDs, however OLND-induced blood oxygenation rapidly decreased, and after only 10 min oxy-Hb levels were similar to those observed before starting the treatment. Transdermal oxygen delivery could be limited by low skin permeability due to the stratum corneum, the outermost layer of the skin.63,64

Notably, US might promote in our system a cascade of events strongly impacting on the oxygen release kinetics, although the actual microscopic events (e.g. nanodroplets vaporization, cell poration, etc.) have to be investigated more deeply. Therefore, the ability of high frequency US to trigger OLND trespassing of the dermal layer and to subsequently enhance oxygen release was tested either in vitro or in vivo. In vitro, US improved the ability of both liquid and gel OLND formulations to cross the pig skin membrane and to

release oxygen into the following hypoxic chamber, being such oxygen release significantly larger than that from OFNDs, OLNBs, OFNBs, and OSS formulations. This experimental evidence was also confirmed in vivo, since US promoted transdermal oxygen delivery through the skin of OLND-treated mice in a time-sustained manner. Sonication appears therefore essential to induce oxygen release from OLNDs after topical treatment.

5. Conclusions

In conclusion, new OLNDs display in vitro a greater capability to deliver oxygen than former OLNBs and OSS. In vivo, US is essential to induce sustained transdermal oxygen delivery from OLNDs. Since US-activated OLNDs appear a very promising device for treating hypoxic wounds, including critical limb ischemia, diabetic foot, and bedsores, preclinical and clinical studies are strongly envisaged.

Acknowledgements

We gratefully acknowledge Compagnia di San Paolo (Ateneo-San Paolo 2011 ORTO11CE8R grant to CG), Università di Torino (ex-60% funds to RC) and Fujifilm Visualsonics for funding support to this work. Thanks are due to Savino Lacerenza for acting as intermediary with Fujifilm Visualsonics and to Monica Argenziano for help with TEM microscopy.

Notes and references

1. D. Mathieu and R. Mani, International Journal of Lower Extremity, 2007, 6, 273–283 CrossRef PubMed .
2. Dietz, S. Jerchel, M. Szaszák, K. Shima and J. Rupp, Microbes Infect., 2012, 14, 311–316 CrossRef CAS PubMed .
3. B. Zbytek, D. L. Peacock, T. N. Seagroves and A. Slominski, Derm.-Endocrinol., 2013, 5, 239–251 CrossRef PubMed .
4. V. W. Wong, G. C. Gurtner and M. T. Longaker, Mayo. Clin. Proc., 2013, 88, 1022–1031 CrossRef PubMed .
5. C. K. Sen, Wound Repair Regen., 2009, 17, 1–18 CrossRef PubMed .
6. Medina, P. G. Scott, A. Ghahary and E. E. Tredget, J. Burn Care Rehabil, 2005, 26, 306–319 CrossRef
7. Schultz, M. Bien, K. Dumond, K. Brown and A. Myers, AORN J, 1999, 70, 434–449 CrossRef CAS .
8. Balakrishnan, T. P. Rak and M. S. Meininger, Burns, 1995, 21, 622–623 CrossRef CAS .
9. Trilla and J. M. Miro, J. Chemother., 1995, 7, 37–43 Search PubMed .
10. E. Eisenbud, Clin. Plast. Surg., 2012, 39, 293–310 CrossRef PubMed .
11. P. Cabrales and M. Intaglietta, ASAIO J., 2013, 59, 337–354 CrossRef CAS PubMed .
12. C. L. Modery-Pawlowski, L. L. Tian, V. Pan and A. Sen Gupta, Biomacromolecules, 2013, 14, 939–948 CrossRef CAS PubMed .
13. C. I. Castro and J. C. Briceno, Artif. Organs, 2010, 34, 622–634 Search PubMed .
14. Bisazza, P. Giustetto, A. Rolfo, I. Caniggia, S. Balbis, C. Guiot and R. Cavalli, Conf. Proc. IEEE Eng. Med. Biol. Soc., 2008, 2008, 2067–2070 Search PubMed .
15. R. Cavalli, A. Bisazza, P. Giustetto, A. Civra, D. Lembo, G. Trotta, C. Guiot and M. Trotta, Int. J. Pharm., 2009, 381, 160–165 CrossRef CAS PubMed .
16. R. Cavalli, A. Bisazza, A. Rolfo, S. Balbis, D. Madonnaripa, I. Caniggia and C. Guiot, Int. J. Pharm., 2009, 378, 215–217 CrossRef CAS PubMed .
17. E. G. Schutt, D. H. Klein, R. M. Mattrey and J. G. Riess, Angew Chem. Int., Ed., 2003, 42, 3218–3235 CrossRef CAS PubMed .

18. J. Y. Fang, C. F. Hung, S. C. Hua and T. L. Hwang, Ultrasonics, 2009, 49, 39–46 CrossRef CAS PubMed
19. Sanfeld, K. Sefiane, D. Benielli and A. Steinchen, Adv. Colloid Interface Sci., 2000, 86, 153–193 CrossRef CAS .
20. E. Lundgren, G. W. Bergoe and I. Tyssebotn, Undersea Hyperbaric Med., 2004, 31, 105–106 CAS .
21. Cavalli, A. Bisazza, M. Trotta, M. Argenziano, A. Civra, M. Donalisio and D. Lembo, Int. J. Nanomed., 2012, 7, 3309–3318 CrossRef CAS PubMed .
22. Cavalli, A. Bisazza and D. Lembo, Int. J. Pharm., 2013, 456, 437–445 CrossRef CAS PubMed .
23. F. Kiessling, Cancer theranostics, ed. X. Chen and S. Wong, Academic Press, Amsterdam, 1st edn, 2014, ch. 10, pp. 127–137, ISBN: 9780124077225 Search PubMed .
24. Guiot, G. Pastore, M. Napoleone, P. Gabriele, M. Trotta and R. Cavalli, Ultrasonics, 2006, 44, e127–e130 CrossRef PubMed .
25. P. Giustetto, A. Bisazza, A. Biagioni, A. Alippi, A. Bettucci, R. Cavalli and C. Guiot, Conf. Proc. IEEE Eng. Med. Biol. Soc., 2008, 2008, 2306–2309 Search PubMed .
26. Park, H. Park, J. Seo and S. Lee, Ultrasonics, 2014, 54, 56–65 CrossRef CAS PubMed .
27. E. Polat, D. Hart, R. Langer and D. Blankschtein, J. Controlled Release, 2011, 152, 330–348 CrossRef CAS PubMed .
28. Lentacker, I. De Cock, R. Deckers, S. C. De Smedt and C. T. Moonen, Adv. Drug. Delivery Rev., 2013, 21 DOI:10.1016/j.addr.2013.11.008 .
29. Kagan, M. J. Benchimol, J. C. Claussen, E. Chuluun-Erdene, S. Esener and J. Wang, Angew. Chem., Int. Ed., 2012, 51, 7519–7522 CrossRef CAS PubMed .
30. J. H. Bang and K. S. Suslick, Adv. Mater., 2010, 22, 1039–1059 CrossRef CAS PubMed .
31. N. Y. Rapoport, D. A. Christensen, H. D. Fain, L. Barrows and Z. Gao, Ultrasonics, 2004, 42, 943–950 CrossRef CAS PubMed .
32. J. Di, J. Price, X. Gu, X. Jiang, Y. Jing and Z. Gu, Adv. Healthcare Mater., 2014, 3, 811–816 CrossRef CAS PubMed .
33. Sze, D. Erickson, L. Ren and D. Li, J. Colloid Interface Sci., 2003, 261, 402–410 CrossRef CAS .
34. P. Boukamp, R. T. Dzarlieva-Petrusevska, D. Breitkreuz, J. Hornung, A. Markham and N. E. Fusenig, J. Cell Biol., 1988, 106, 761–771 CrossRef CAS .
35. De Backer, K. Donadello and D. O. Cortes, J. Clin. Monit. Comput., 2012, 26, 361 CrossRef PubMed .
36. G. Cumming, F. Fidler and D. L. Vaux, J. Cell Biol., 2007, 177, 7–11 CrossRef CAS PubMed .
37. M. P. Krafft and J. G. Riess, Biochimie, 1998, 80, 489–514 CrossRef CAS .
38. J. G. Riess and M. P. Krafft, Mater. Res. Soc. Bull., 1999, 24, 42–48 CrossRef CAS .
39. V. P. Hoven, V. Tangpasuthadol, Y. Angkitpaiboon, N. Vallapa and S. Kiatkamjornwong, Carbohydr. Polym., 2007, 68, 44–53 CrossRef CAS PubMed .
40. S. K. Shukla, A. K. Mishra, O. A. Arotiba and B. B. Mamba Int, J. Biol. Macromol., 2013, 59, 46–58 CrossRef CAS PubMed .
41. J. H. Park, Y. W. Cho, H. Chung, I. C. Kwon and S. Y. Jeong, Biomacromolecules, 2003, 4, 1087–1091 CrossRef CAS PubMed .
42. P. Zhang and M. Cao, Int. J. Biol. Macromol., 2014, 10 DOI:10.1016/j.ijbiomac.2014.01.009 .
43. L. Harkins, S. Duri, L. C. Kloth and C. D. Tran, J. Biomed. Mater. Res., Part B, 2014, 10 DOI:10.1002/jbm.b.33103 .
44. Y. W. Cho, Y. N. Cho, S. H. Chung, G. Yoo and S. W. Ko, Biomaterials, 1999, 20, 2139–2145 CrossRef CAS .
45. J. Y. Je, Y. S. Cho and S. K. Kim, Bioorg. Med. Chem. Lett., 2006, 16, 2122–2126 CrossRef CAS PubMed .
46. S. Lee, S. Y. Jeong, Y. M. Kim, M. S. Lee, C. B. Ahn and J. Y. Je, Bioorg. Med. Chem., 2009, 17, 7108–7112 CrossRef CAS PubMed .
47. A. Tayel, S. Moussa, W. F. el-Tras, D. Knittel, K. Opwis and E. Schollmeyer, Int. J. Biol. Macromol., 2010, 47, 454–457 CrossRef CAS PubMed .

48. M. M. Abdel-Mottaleb, B. Moulari, A. Beduneau, Y. Pellequer and A. Lamprecht, J. Pharm. Sci., 2012, 101, 4231–4239 CrossRef CAS PubMed .
49. R. F. Lopez, J. E. Seto, D. Blankschtein and R. Langer, Biomaterials, 2011, 32, 933–941 CrossRef CAS PubMed .
50. X. Wu, K. Landfester, A. Musyanovych and R. H. Guy, Skin Pharmacol. Physiol., 2010, 23, 117–123 CrossRef CAS PubMed .
51. Y. Chen, L. Zhou, L. Yuan, Z. H. Zhang, X. Liu and Q. Wu, Int. J. Nanomed., 2012, 7, 3023–3032 CAS .
52. J. L. Minkin and A. S. Kellerman, Public Health Rep., 1966, 81, 875–884 CrossRef CAS .
53. J. C. Chang, S. F. Ossoff, D. C. Lobe, M. H. Dorfman, C. M. Dumais, R. G. Qualls and J. D. Johnson, Appl. Environ. Microbiol., 1985, 49, 1361–1365 CAS .
54. Chatzisymeon, A. Droumpali, D. Mantzavinos and D. Venieri, Photochem. Photobiol. Sci., 2011, 10, 389–395 CAS .
55. J. Weber and W. A. Rutala, Am. J. Infect. Control, 2013, 41, S31–S35 CrossRef PubMed .
56. Fenoglio, J. Ponti, E. Alloa, M. Ghiazza, I. Corazzari, R. Capomaccio, D. Rembges, S. Oliaro-Bosso and F. Rossi, Nanoscale, 2013, 5, 6567–6576 RSC .
57. T. P. Devasagayam and J. P. Kamat, Indian J. Exp. Biol., 2002, 40, 680–692 CAS .
58. T. A. Mustoe, K. O'Shaughnessy and O. Kloeters, Plast. Reconstr. Surg., 2006, 117, 35S–41S CrossRef CAS PubMed .
59. Y. P. Xia, Y. Zhao, J. W. Tyrone, A. Chen and T. A. Mustoe, J. Invest. Dermatol., 2001, 116, 50–56 CrossRef CAS PubMed .
60. J. Jose, R. G. Willemink, S. Resink, D. Piras, J. C. van Hespen, C. H. Slump, W. Steenbergen, T. G. van Leeuwen and S. Manohar, Opt. Express, 2011, 19, 2093–2104 CrossRef PubMed .
61. S. Resink, J. Jose, R. G. Willemink, C. H. Slump, W. Steenbergen, T. G. van Leeuwen and S. Manohar, Opt. Lett., 2011, 36, 2809–2811 CrossRef PubMed .
62. J. Laufer, D. Delpy, C. Elwell and P. Beard, Phys. Med. Biol., 2007, 52, 141–168 CrossRef CAS PubMed
63. Naik, Y. N. Kalia and R. H. Guy, Pharm. Sci. Technol. Today., 2000, 3, 318–326 CrossRef CAS .
64. S. H. Lee, S. K. Jeong and S. K. Yonsei, Med. J., 2006, 47, 293–306 CAS .